fNIRS Evidence for Distinguishing Patients With Major Depression and Healthy Controls

Jinlong Chao, *Graduate Student Member, IEEE*, Shuzhen Zheng, Hongtong Wu, *Graduate Student Member, IEEE*, Dixin Wang, *Graduate Student Member, IEEE*, Xuan Zhang, *Associate Member, IEEE*, Hong Peng, *Member, IEEE*, and Bin Hu, *Senior Member, IEEE*

***Abstract*— In recent years, major depressive disorder (MDD) has been shown to negatively impact physical recovery in a variety of patients. Functional near-infrared spectroscopy (fNIRS) is a tool that can potentially supplement clinical interviews and mental state examinations to establish a psychiatric diagnosis and monitor treatment progress. Thirty-two subjects, including 16 patients clinically diagnosed with MDD and 16 healthy controls (HCs), participated in the study. Brain oxyhemoglobin (HbO) and deoxyhemoglobin (HbR) responses were recorded using a 22-channel continuous-wave fNIRS device while the subjects performed the emotional sound test. This study evaluated the difference between MDD patients and HCs using a variety of methods. In a comparison of the Pearson correlation coefficients between the HbO/HbR responses of each fNIRS channel and four scores, MDD patients and HCs had significantly different Athens Insomnia Scale (AIS) scores. By quantitative evaluation of the functional association, we found that MDD patients had aberrant functional connectivity compared with HCs. Furthermore, we concluded that compared with HCs, there were marked abnormalities in blood oxygen in the bilateral ventrolateral prefrontal cortex (VLPFC) and bilateral dorsolateral prefrontal cortex (DLPFC). Four statistical-based features extracted from HbO signals and four vector-based features from both HbO and HbR served as inputs to four simple neural networks (multilayer neural network (MNN), feedforward neural network (FNN), cascade forward neural network (CFNN) and recurrent neural network (RNN)). Through an analysis of combinations of different features, the combination of 4 common features (mean, STD, area under the receiver operating characteristic curve (AUC) and slope) yielded the highest classification accuracy of 89.74% for fear emotion. The combination of four novel feature (*CBV*, *COE*, $|L|$ and K) resulted in a classification accuracy of 99.94% for fear emotion. The top 10 common and novel features were selected by the ReliefF feature selection algorithm, resulting in classification accuracies of 83.52% and 91.99%, respectively. This study identified the AUC and angle K as specific neuromarkers for predicting MDD across specific depression-related regions of the prefrontal cortex (PFC). These findings suggest that the fNIRS measurement of the PFC may serve as a supplementary test in routine clinical practice to further support a diagnosis of MDD.**

***Index Terms*— Functional near-infrared spectroscopy (fNIRS), major depressive disorder (MDD), activation patterns, simple neural networks, feature selection.**

Manuscript received April 16, 2021; revised August 15, 2021; accepted September 17, 2021. Date of publication September 23, 2021; date of current version November 2, 2021. This work was supported in part by the National Key Research and Development Program of China under Grant 2019YFA0706200 and in part by the National Natural Science Foundation of China under Grant 61632014, Grant 61627808, and Grant 61210010. *(Corresponding authors: Bin Hu; Hong Peng.)*

This work involved human subjects or animals in its research. Approval of all ethical and experimental procedures and protocols was granted by GuangYuan Mental Health Center Ethics Committee under Application No. GJWLSP2020012, and performed in line with the Ethical Review Measures for Biomedical Research Involving Human Subjects, Declaration of Helsinki, and International Ethical Guidelines for Biomedical Research Involving Human Subjects.

Jinlong Chao, Shuzhen Zheng, Hongtong Wu, Dixin Wang, Xuan Zhang, and Hong Peng are with the School of Information Science and Engineering, Lanzhou University, Lanzhou 730000, China (e-mail: chaojl18@lzu.edu.cn; zhengsz_lzu@163.com; wuht2020@lzu.edu.cn; wangdx20@lzu.edu.cn; zhangxuan20@lzu.edu.cn; pengh@lzu.edu.cn).

Bin Hu is with Gansu Provincial Key Laboratory of Wearable Computing, School of Information Science and Engineering, Lanzhou University, Lanzhou 730000, China, and also with CAS Center for Excellence in Brain Science and Institutes for Biological Sciences, Shanghai Institutes for Biological Sciences, Chinese Academy of Sciences, Shanghai 200031, China (e-mail: bh@lzu.edu.cn).

Digital Object Identifier 10.1109/TNSRE.2021.3115266

I. Introduction

With the accelerated pace of life and the increasingly fierce social competition, people's psychological pressure is gradually increasing, and the incidence of depression is increasing annually. According to the World Health Organization, the worldwide prevalence of depression is approximately 3%-5% (approximately 100 to 200 million people) [1]. By 2022, depression will become the most serious disease burden in developing countries, and major depressive disorder (MDD) will become the second leading cause of suicide and disease [2], [3]. Due to the lack of specific diagnostic methods for depression and its various manifestations, accurate and reliable diagnosis of depression mainly depends on the clinical skills and clinical judgment of psychologists [4], [5]. The comprehensive collection of accurate and reliable medical history and careful psychophysiological examination are the basis for diagnosis. Therefore, detecting depression early through physiological indicators is becoming increasingly important.

Brain imaging technology has allowed researchers to noninvasively detect brain activity during a depressive state [6], [7], and many imaging technologies, including electroencephalography (EEG) [8], [9], magnetoencephalography (MEG) [10], functional magnetic resonance imaging (fMRI) [11], and

positron emission tomography (PET) [12], have been widely used to explore the mechanism of abnormal brain activity in depression and other mental illnesses. Neural activity provides better information for emotion recognition due to its higher specificity for different types of emotions [13], [14]. Researchers have tried to develop objective biological criteria for the diagnosis of depression and targeted treatment.

Jobsis [15] first reported a noninvasive infrared method of monitoring cerebral oxygen sufficiency. Functional near-infrared spectroscopy (fNIRS) is a noninvasive, safe, low cost, and portable optical brain imaging technique that has been recently proposed as a potential diagnostic method for detecting MDD [16]. Because it can objectively reflect the state of brain activity, it is currently an effective tool for the auxiliary diagnosis of depression. Currently, the application of fNIRS in rehabilitation and medical care is limited; however, this approach has high potential.

In recent years, a significant amount of research on MDD based on fNIRS has been widely performed, and these studies have shown the great potential of neural-signal-based MDD recognition [2], [17]. A recent analysis assessing depression pre- and post-treatment showed a consistent wave pattern, which led to the response in the frontal cortex being regarded as a trait marker [18]. In such studies, the verbal fluency task (VFT) is the most widely used paradigm. Liu *et al.* [19] found that a brain oxyhemoglobin (HbO) concentration change in the bilateral prefrontal cortex (PFC) and anteromedial PFC was associated with depression severity. Moreover, Akashi *et al.* [20] found that the mean HbO changes induced by a VFT were significantly smaller in patients with MDD than in healthy controls (HCs). In [21] and [22], patients with MDD had smaller changes in HbO in the frontal and temporal cortices than HCs. In addition, Toshio Matsubara [23] found that different neural circuits play a role in emotional processing in MDD patients and HCs. Regarding the MDD classification research, Zhu *et al.* [24] used a wearable fNIRS head probe monitoring specific brain regions, and limiting extraction to a few features (mean HbO, full width at half maximum and kurtosis) resulted in a classification accuracy of 92.6%, a sensitivity of 84.8%, and a specificity of 91.7% using the XGBoost classifier. In [25], 36 MDD patients and 48 bipolar depression (BD) patients were monitored by fNIRS while conducting the VFT, and the average classification accuracy reached 96.2%. Additionally, in [26], 20 participants (10 MDD patients and 10 HCs) were instructed to perform submaximal isometric handgrip force control tasks, and the best performance predictive model had an accuracy of 85%.

The analysis methods of these studies are too simple to fulfill all the diagnostic requirements, and similar paradigms are used. Usually, only the blood oxygen levels of MDD patients and HCs are studied. To solve these problems, different paradigms and more comprehensive analysis methods need to be implemented to assess the MDD state. Regarding MDD classification studies, numerous studies have the problems of a single feature type and low accuracy. Therefore, instability of the classification accuracy in MDD recognition is seriously detrimental to the normal use of fNIRS-based brain-computer interfaces (BCIs) [27] and renders their deployment for treatment or rehabilitation less likely [28], [29].

Focusing on this issue, we used fNIRS measurements and conducted fNIRS sound induction experiments to explore whether consistent, reproducible and typical prefrontal activation patterns exist in patients with MDD compared with HCs. In this study, we used 22 fNIRS channels covering the PFC region. Four different methods, namely, correlation analysis of an oxygen index and a scale, resting-state analysis, activation analysis and simple neural network recognition, were used for quantitative classification of MDD patients. Through the comparison of two different types of features, the feature dimensions were reduced to 10 by feature selection. Our study suggests fNIRS measurement of the PFC as a potential biomarker for auxiliary diagnosis of MDD. The contributions of this study are as follows:

(1) Several methods, including correlation analysis of the oxygen index (HbO) of each individual fNIRS channel and the scales (PHQ-9, PHQ-15, GAD-7 and AIS), resting-state analysis and activation analysis were applied in our study. It provides some neuroscience evidence for our subsequent classification.
(2) An emotional sound test was conducted, during which 32 fNIRS signals (from 16 MDD patients and 16 HCs) were recorded. Two types of features, namely, statistical-based and vector-based features, were extracted from the dataset. Moreover, the optimum feature matrix was constructed for depression classification by the feature selection method. The number of channels and the computational complexity were reduced.
(3) Four simple neutral networks were evaluated and verified using leave-one-subject-out (LOSO) scenario, and good results were obtained.

The structure of this paper is as follows. In section II, we describe the participants, experimental paradigm, optode placement, data collection method, fNIRS data preprocessing method, correlation analysis of the oxygen index and scales, resting-state analysis and activation analysis used in this study. In section III, we present the methods of feature extraction and selection. The results and an accuracy comparison are reported in section IV. Finally, we present a discussion in section V.

II. Materials and Methods

A. Participants

In this study, through strict screening, matching, and effective data collation, 32 participants with no history of any neurological disorder participated in the experiment, including 16 MDD patients and 16 HCs. The MDD patients recruited in this study were from the psychiatric department of the Tianshui Third Hospital, Gansu, China. This study was approved by the local research ethics committee, and written informed consent from all subjects was obtained after explaining the experimental paradigm in detail.

All the MDD subjects were selected by professional psychiatrists using the Mini-Mental State Examination (MMSE). The relevant basic information statistics were analyzed for the subjects. The Patient Health Questionnaire-9 (PHQ-9) and

TABLE I
DEMOGRAPHIC CHARACTERISTICS; PHQ-9, PHQ-15, AIS, GAD-7 SCORES; AND GROUP DIFFERENCE RESULTS OF THE MDD PATIENTS AND HCS (MEAN±STD)

Characteristic	MDD	HC	Group difference (p-value)
Age	35.5 ± 9.0	36.2 ± 11.7	N/A
Sex (female/male)	12F/4M	10F/6M	N/A
Education (years)	9. 68 ± 3.19	9.32 ± 3.51	N/A
PHQ-9 score	13.56 ± 6.30	3.75 ± 5.04	**<0.001**
PHQ-15 score	11.25 ± 4.92	4.81 ± 3.54	**<0.001**
GAD-7 score	11.19 ± 5.36	3.85 ± 4.57	**<0.001**
AIS score	15.31 ± 4.74	5.44 ± 4.29	**<0.001**

(PHQ=Patient Health Questionnaire, GAD=Generalized Anxiety Disorder, AIS= Athens Insomnia Scale)

Patient Health Questionnaire-15 (PHQ-15) were used to assess the degree of depression. The Generalized Anxiety Disorder-7 (GAD-7) is a tool for screening and measuring the severity of anxiety, and we used this scale to distinguish depression from anxiety. The t-test was used to evaluate the education level. The results are shown in Table I. The statistical results showed that there were no statistically significant sex and education level differences between the two groups. The MDD group showed higher scores on the PHQ-9, PHQ-15, and GAD-7 compared with the HCs.

B. Experimental Paradigm

Various brain activities, such as motor imagery, motor execution, word generation, object rotation, mental arithmetic, music imagery, letter padding, motor execution and other visual tasks, have been used by fNIRS researchers in the literature [30]. In this study, the above diagram illustrates the areas of the PFC in which HbO, deoxyhemoglobin (HbR) and total hemoglobin (HbT) changes were studied. We conducted a sound stimuli paradigm, as shown in Fig. 1. The audio material was carefully obtained from selected files. After verification in multiple subjects, significant differences were found in the valence and arousal of each audio stimulus. Before the experiment was conducted, subjects were evaluated in groups, and uniform instructions were provided. Specifically, all the subjects were given a mini lesson by the tester, in which the precautions and requirements of the experiment were explained. This experiment was divided into two parts: resting-state fNIRS recording and task-relevant fNIRS recording. In the resting-state recording session, all the subjects needed to close their eyes and remain conscious for 3 minutes. There was a "ding" prompt at the beginning and end and a prompt in the middle of the screen during the audio stimulus.

For the task-relevant session, the experiment consisted of 16 trials and was divided into four blocks; each block consisted of 4 types of sound stimuli, played in a Latin square design. For each trial, an affective sound stimulus was played into the subject's ears through earphones for 18 s. After each trial, the subject was given 20 s of rest to allow the hemodynamic response to return to baseline. When

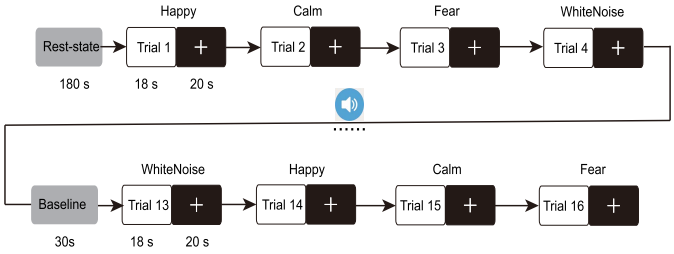

Fig. 1. Experimental paradigm for data acquisition. After the initial 180-s resting state, a single trial consisted of 18 s of a sound stimuli task followed by 20 s of rest, then 18 s of a sound stimuli task again followed by 20 s of rest. In total, 16 trials were recorded, corresponding to a complete experimental duration of 878 s.

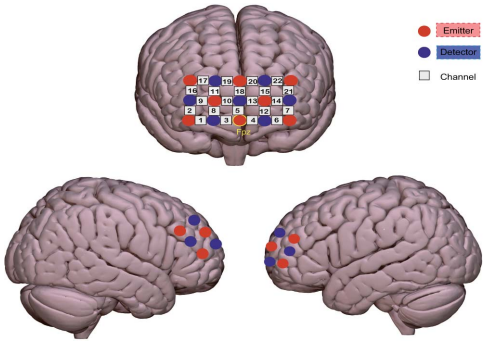

Fig. 2. Measurement points of the 22 fNIRS channels. Red and blue diamond's represent emitters and detectors, respectively. In total, eight emitters and seven detectors, with a separation of 3 cm between each emitter-detector pair, yielded 22 channels to record the brain signals. The 22 measured positions are labeled channel (Ch) 1 to Ch (22), from the right to left sides of the PFC.

all 16 segments of stimulation were played, the experiment was completed. The total duration of the experiment was approximately 15 minutes. Subjects were asked to restrict their body movements during the experiment as much as possible.

C. Channel Configuration and Optode Placement

Regarding the measured fNIRS signals from the PFC, the measured brain regions were not consistent with those of past studies [31]. In this study, the fNIRS system was equipped with 8 sources and 7 detectors according to the 10-20 international system, and the distance between each pair of sources and detectors was set to 3 cm. The measurement area between each pair was defined as a channel (Ch). In total, 22 channels were recorded in this study. Fig. 2 shows the emitter-detector arrangement on the PFC.

D. Data Collection

fNIRS signals from the PFC were acquired using a multichannel continuous-wave (CW) NIRScout fNIRS system (NIRx Medical Technologies, LLC). The optode placement configuration was recorded in the NIRStar data acquisition software (version 15.1). The brain imaging system used two wavelengths, 760 and 850 nm, and the sampling frequency was 7.81 Hz. In our study, an elastic measurement headband (20 × 8 cm) was mounted over the PFC of each subject's head;

the total fNIRS setup time required to place the headband was approximately 8 minutes.

E. Data Preprocessing

The NIRS data were processed on a channel-by-channel basis using the HOMER2 [32] toolbox. The raw optical signal is recorded as a time series of optical intensity values for each channel, so the intensity data needed to be converted to concentrations of HbO, HbR and HbT. The changes in the concentrations of HbO and HbR due to neuronal activity can be calculated using the modified Beer-Lambert law (MBLL) [33].

The acquired hemodynamic signal contains various types of noise, such as instrumental, physiological and experimental noise, which should be removed before further processing [34]. First, for identification of motion artifacts, if any active data channel exhibits a signal change of greater than the STD or AMP threshold, then the segment of data around that time point is marked as a motion artifact. The specific parameters are set to t Motion=0.5, t Mask=3.0, STD threshold=20.0, and AMP threshold=5.0. Then, we perform a spline interpolation for motion artifact correction. The spline interpolation results depend on interpolation parameter p, and p spline=0.99 is believed to be effective in removing motion artifacts [35], [36]. Finally, we use a 2nd-order Butterworth bandpass filter with a cutoff frequency of 0.01-0.2 Hz to remove physiological noise due to heartbeat (>1 Hz), respiration (approximately 0.2-0.5 Hz), and high-frequency noise [16], [37]. In our study, signal preprocessing was performed using the HOMER2 toolbox in MATLAB 2013b (MathWorks, Inc.; Natick, US).

F. Correlation Analysis of the Oxygen Index and Depression Scales

The objective was to explore the characteristics of the oxygen index and its relationships with depression scale scores. This relationship between the HbO index of each individual fNIRS channel and the depression scales was characterized by computing the Pearson correlation coefficients, and a significance level of 5% was considered.

G. Resting-State Analysis

The brain functional networks are mainly composed of edges and nodes. First, we defined the fNIRS channel positions as the nodes of the brain network; the number of nodes was 22. Moreover, the definition of the edge is based on the calculated connectivity between the channels. In this study, we selected three coupling methods, including Pearson's correlation coefficient (CORR), the magnitude squared coherence (COH) and phase-locking value (PLV), to calculate the functional connectivity matrixes. The formulas are shown in Table II.

$CORR_{xy}$ is a measurement used to describe the linear correlation between two channels. COH_{xy} is the square of the coherency function (K), $P_{xy}(f)$ is the covariance of the two channels at frequency f, and $P_{xx}(f)$ and $P_{yy}(f)$ are the power spectra of the two channels at frequency f. The PLV index considers only the relative phase difference of two channels, and it is not affected by the amplitude.

TABLE II
MATHEMATICAL FORMULATION OF THE THREE COMPUTING METHODS USED IN THIS STUDY

Method	Mathematical formulation
CORR	$CORR_{xy} = \frac{1}{N}\sum_{k=1}^{N} x(t)y(t)$
COH	$COH_{xy} = k_{xy}^2(f) = \lvert K_{xy}(f)\rvert^2 = \frac{\lvert MeanP_{xy}(f)\rvert^2}{MeanP_{xx}(f)MeanP_{yy}(f)}$
PLV	$PLV = \left\lvert e^{i\Delta\phi_{rel}(t)}\right\rvert = \left\lvert \frac{1}{N}\sum_{n=1}^{N} e^{i\Delta\phi_{rel}(t_n)}\right\rvert = \sqrt{cos\Delta\phi_{rel}(t)^2 + sin\Delta\phi_{rel}(t)^2}$

The connectivity matrix is represented by an N × N square matrix, where the rows and columns represent the nodes in the connectivity network. The nodes can be represented by channels or the region of interest (RoI). The value in the connectivity matrix represents the strength of the connectivity between nodes.

H. Activation Analysis

Task activation was quantified by a statistical parametric mapping approach based on a generalized linear model (GLM) [38]. In Equation (1), Y is the vector of measurements, X is the design matrix encoding the timing of stimulus events, and regression coefficients β_i are weighted values of the stimulus condition for the corresponding channel. This method fits the fNIRS data with a linear combination of explanatory variables that reflect the design of the stimulus. Thus, the GLM has a higher statistical power than the mean because it considers the entire fNIRS time series. In this study, parameter β is the eigenvalue extracted to discriminate the patients with MDD and the HCs. Only those channels that were found to have significant activation ($p<0.05$) were included in this study [39].

$$\begin{bmatrix} Y_1 \\ Y_2 \\ \vdots \\ Y_n \end{bmatrix} = \begin{bmatrix} 1 & X_{11} & \cdots & X_{1p} \\ 1 & X_{21} & \cdots & X_{2p} \\ \vdots & \vdots & & \vdots \\ 1 & X_{np} & \cdots & X_{np} \end{bmatrix} \times \begin{bmatrix} \beta_0 \\ \beta_1 \\ \vdots \\ \beta_p \end{bmatrix} + \begin{bmatrix} \varepsilon_1 \\ \varepsilon_2 \\ \vdots \\ \varepsilon_n \end{bmatrix} \quad (1)$$

Once these values were obtained, we used these values and Montreal Neurological Institute (MNI) coordinates to locate the specific activation channel. The Nirs2img function was used to construct .img and .hdr documents, and these overlays were then added to the cerebra model achieved by Surf_Ice software. Surf_Ice is a tool used for rendering the cortex with overlays to illustrate the tractography, network connections, anatomical atlases and statistical maps. In this study, we use this method to render the activation mode.

III. FEATURE EXTRACTION AND SELECTION

A. Statistical-Based Feature Extraction

Statistical features are conventionally used to extract information from data [40], [41]. The purpose of including these features in the current study was to compare the performance of the proposed method against that of these conventionally used features. Four common statistical features (mean, STD,

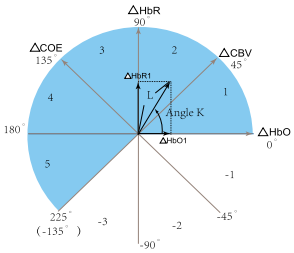

Fig. 3. Polar coordinate plane for the analysis of cerebral oxygenation. Phase numbers are shown in each octant. The relationship between the cerebral oxygen change (ΔCOE) and cerebral blood volume (ΔCBV) can be detected by the trajectory of a vector.

area under the receiver operating characteristic curve (AUC) and slope) were calculated for ΔHbO. The temporal statistical features were aggregated using a statistic for each trial and channel.

In our study, each trial had 18 s of task-related data points, and only 0-7 s of data points were extracted in the study; therefore, we had a total of 8 trials for positive and negative conditions. The total number of samples were 16 $(subjects) \times 4$ $(trials) \times 2$ $(MDD + HC) = 128$. Four attributes (mean, STD, AUC and slope) from all 22 channels were obtained, yielding $4 \times 22 = 88$ channels of vector features, from Ch1_Mean, Ch2_Mean... to Ch21_Slope, Ch22_Slope. Therefore, the final feature vector using the statistical-based features has dimensions of 128×88.

B. Vector-Based Feature Extraction

Vector-based phase analysis has been successfully used for the detection of initial dips in fNIRS signals [30], [42], [43]. This method is based on an orthogonal vector coordinate plane defined by ΔHbO and ΔHbR signals, and rotating this plane by 45 degrees counterclockwise results in another orthogonal plane defined by ΔCBV and ΔCOE. A positive value for ΔCOE shows a hypoxic change starting from ΔCOE=0, and a negative value for ΔCOE shows a hyperoxic change. The polar coordinate plane formed from these four axes is called a cerebral oxygen regulation (CORE) vector plane. A CORE vector has the four hemoglobin indices ΔHbO, ΔHbR, ΔCBV and ΔCOE as its components, and the relationship between them is shown in Fig. 3.

The angle k represents the ratio of ΔCOE to ΔCBV and indicates the degree of oxygen exchange. The magnitude $|L|$, drawn from the origin of a CORE vector to the coordinates of a cumulative sum, shows the amplitude of a CORE vector and represents the amount of change in hemoglobin.

The formulas are defined in Table III.

The four attributes of the vector-based phase analysis given in Table III are computed for each time point of ΔHbO and ΔHbR. In our study, each trial had 140 data points, and we had a total of 8 trials for positive and negative conditions. Therefore, the total number of data samples were 140 $(data\ points) \times 16$ $(subjects) \times 4$ $(trials) \times 2$ $(MDD + HC) = 17920$. Four attributes (ΔCBV, ΔCOE, $|L|$ and K) from all 22 channels were obtained, yielding $4 \times 22 = 88$ channels of vector-based features from Ch1_ΔCBV and Ch2_ΔCBV... to Ch21_K and CH22_K. Therefore, the final feature vector using the vector-based features has dimensions of $17,920 \times 88$.

TABLE III
DESCRIPTION OF VECTOR-BASED FEATURES

No.	Novel features	Dimensions	Mathematical formulation
1	ΔCBV	22	$\Delta CBV = \frac{(\Delta HbO + \Delta HbR)}{\sqrt{2}}$
2	ΔCOE	22	$\Delta COE = \frac{(\Delta HbR - \Delta HbO)}{\sqrt{2}}$
3	Magnitude of vector $\|L\|$	22	$\|L\| = \frac{\sqrt{(\Delta HbO^2 + \Delta HbR^2)}}{\sqrt{2}}$
4	Angle K	22	$K = tan^{-1}(\frac{\Delta COE}{\Delta CBV})$

C. Feature Selection

ReliefF is a type of feature weighting algorithm [44]. According to the correlation between each feature and category, different weights are given to the features, and the features whose weights are less than a certain threshold are removed. This correlation is a measure of the distance between the feature and its nearest samples. The weight of each feature was determined by this distance. Therefore, the larger the weight, the stronger the classification ability of the feature, and vice versa. In this study, the ReliefF algorithm was used for feature selection. For statistical- and vector-based features, we selected the top 10 features for later classification.

IV. RESULTS AND ANALYSIS

A. Correlation Analysis of the Oxygen Index and Scales

The correlation between the oxygen index (MDD: HbO, HCs: HbO) and the scales (PHQ-9, PHQ-15, GAD-7 and AIS) was analyzed by Pearson correlation coefficients, and we obtained some significant results. The statistical tests were performed at the channel-based level. False discovery rate (FDR) correction was used for the channels with significant results, and p-values below 0.05 were considered to indicate statistically significant differences. The results were as follows: under the happy condition, correlation results of more channels were found in both the MDD and HC groups, as shown in Table IV.

Notably, we found that under the happy condition, the HbO concentration in the MDD group was correlated with the AIS scale for the most channels, namely, Ch1, Ch3, Ch4, Ch10, Ch12, Ch15, Ch16, Ch17, and Ch19. Additionally, all the results were negatively correlated, i.e., the higher the value of the AIS scale score is, the lower the blood oxygen level of MDD patients. The primary reason for this result is that MDD patients often have refractory sleep disorders, and the incidence rate is as high as 98% [45]. Furthermore, some studies have shown that more than 70% of chronic insomnia patients have hypoxemia, resulting in brain excitability due to hypoxia, which leads to insomnia [46]. In the HC group, there was negative correlation of some channels with the PHQ9 (Ch3, Ch5, Ch8, Ch9, Ch10, Ch17) and PHQ15 (Ch3, Ch8, Ch9, Ch10, Ch22).

TABLE IV
STATISTICAL RESULTS OF HBO CONCENTRATION DIFFERENCES BETWEEN MDD PATIENTS AND HCS UNDER HAPPY CONDITIONS

MDD		HC	
PHQ9	(Ch2) R = 0.259*	PHQ9	(Ch3) R = -0.276*
GAD7	(Ch5) R = 0.261*		(Ch5) R = -0.289*
PHQ15	(Ch19) R = -0.382**		(Ch8) R = -0.289*
AIS	(Ch1) R = -0.357**		(Ch9) R = -0.268*
	(Ch3) R = -0.352*		(Ch10) R = -0.321**
	(Ch4) R = -0.330**		(Ch17) R = -0.272*
	(Ch10) R = -0.318**	PHQ15	(Ch3) R = -0.275*
	(Ch12) R = -0.288*		(Ch8) R = -0.270*
	(Ch15) R = -0.267*		(Ch9) R = -0.355**
	(Ch16) R = -0.454**		(Ch10) R = -0.257*
	(Ch17) R = -0.299*		(Ch22) R = -0.250*
	(Ch19) R = -0.424**		

*P<0.05, **P<0.01, FDR correction.

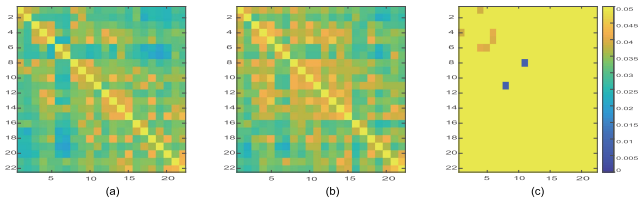

Fig. 4. Functional connectivity matrixes calculated by the CORR. (a) Functional connectivity matrixes of the HC group; (b) functional connectivity matrixes of the MDD group; (c) difference matrix between the two groups filtered out by a t-test ($P < 0.05$).

Under the fear condition, the HC group showed the most channel correlation with the PHQ15 scale, and the results were as follows: PHQ15: (Ch6) R = 0.385**, (Ch7) R = 0.345**, (Ch12) R = 0.271*, (Ch13) R = 0.253*, (Ch15) R = 0.258*, (Ch18) R = 0.277*, (Ch19) R = 0.357*, (Ch21) R = 0.269* and (Ch22) R = 0.365**. Under the calm and white noise conditions, the HbO concentrations of MDD patients and HCs did not appear significant for all channels.

To summarize the above results, we concluded that the MDD group was significantly correlated with the AIS. Furthermore, we speculate that the reason for this finding may be that people with MDD do not want to reflect their true emotional state, and these scale questions often infringe on their privacy. However, for the AIS, they are more willing to describe their real situations. Our study showed a negative correlation between the MDD patients and the assessed scales [47], [48].

B. Resting-State Analysis

We calculated the CORR, COH and PLV connectivity matrix of the MDD and HC groups. The results are shown in Figs. 4-6. Among them, the blue area indicates a more active node (smaller p-value), which shows that it has a higher relevance or synchronization level, and the yellow area indicates a lower degree of relevance between channels.

Fig. 4 (a) and 4 (b), which represent the HC and MDD groups, respectively, show that the yellow area for the MDD group is larger than that of the HC group. The difference

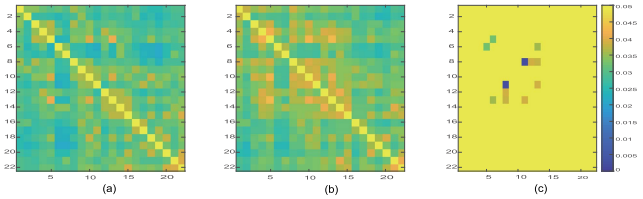

Fig. 5. Functional connectivity matrixes calculated by the COH. (a) Functional connection matrixes of the HC group; (b) functional connectivity matrixes of the MDD group; (c) difference matrix between the two groups filtered out by a t-test ($P < 0.05$).

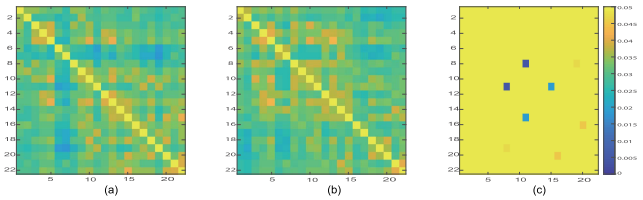

Fig. 6. Functional connectivity matrixes calculated by the PLV. (a) Functional connectivity matrixes of the HC group; (b) functional connectivity matrixes of the MDD group; (c) difference matrix between the two groups filtered out by a t-test ($P < 0.05$).

matrix between the two groups was filtered out by a t-test ($P < 0.05$). Fig. 4 (c) shows the obvious difference in the functional connectivity matrixes of the two groups measured by the CORR. Four significant results were found: Ch1–Ch4 ($P = 0.038$), Ch5–Ch6 ($P = 0.039$), Ch4–Ch6 ($P = 0.040$) and Ch8–Ch11 ($P = 0.008$).

By the same method, Fig. 5 (c) shows the obvious difference in the functional connectivity matrixes of the two groups measured by the COH. Six significant results were found: Ch5–Ch6 ($P = 0.031$), Ch6–Ch13 ($P = 0.036$), Ch8–Ch13 ($P = 0.038$), Ch8–Ch12 ($P = 0.039$), Ch8–Ch11 ($P = 0.003$) and Ch3–Ch11 ($P = 0.004$). Fig. 6 (c) shows the obvious difference in the functional connectivity matrixes of the two groups measured by the PLV. Four significant results were obtained: Ch8–Ch11 ($P = 0.004$), Ch11–Ch15 ($P = 0.019$), Ch8–Ch19 ($P = 0.047$) and Ch16–Ch20 ($P = 0.045$).

Fig. 4 (c), Fig. 5 (c) and Fig. 6 (c) suggest that the functional connectivity matrix constructed by the COH has a higher overall level of relevance or synchronization [49], [50], and its significant result is larger than those of the CORR and PLV. MDD patients have been shown to have aberrant brain function.

C. Activation Analysis

Previous fNIRS studies revealed that positive and negative emotion activation occurs in the PFC [20], [23], [47], [51]. Our study used emotional sound stimuli to induce happiness-calm-fear emotion states in the MDD and HC groups. Statistical analysis of group variables indicated that the HbO concentration of the MDD group was significantly higher than that of the HC group under the happy condition ($P = 0.014$, $t = 2.57$), the HbO concentration in the MDD group under the calm condition was significantly higher than that in the HC group ($P = 0.001$, $t = 3.69$), and the HbO concentration in the MDD group under the fear condition was significantly lower than that in the HC group ($P = 0.001$, $t = -3.50$). There was

TABLE V
SIGNIFICANT DIFFERENCE IN THE HbO CONCENTRATION BETWEEN MDD PATIENTS AND HCs UNDER DIFFERENT CONDITIONS

	Happy	Calm	Fear	White Noise
MDD (N=22)	0.19± 0.20	0.75±0.28	0.57± 0.21	0.74±0.21
HC (N=22)	0.06±0.13	0.46±0.25	0.78±0.19	0.70±0.24
t	2.57*	3.69**	-3.50**	0.64

*P<0.05, **P<0.01
Post hoc P-values are Bonferroni-corrected for multiple comparisons.

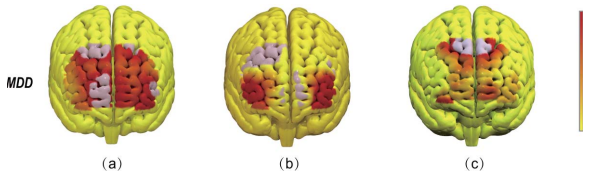

Fig. 7. HbO changes in the MDD patients under (a) happiness, (b) calm, and (c) fear conditions.

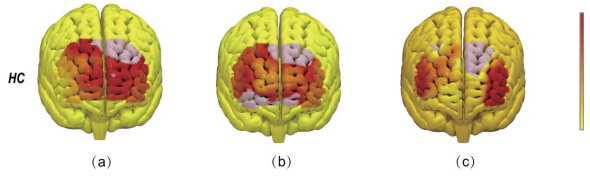

Fig. 8. HbO changes in the HC group under (a) happiness, (b) calm and (c) fear conditions.

no significant difference in HbO concentration between the two groups under the white noise condition ($P > 0.05$). The specific results are shown in Table V.

Fig. 7. shows the frontal lobe activation of MDD patients under three conditions, and the activation patterns show obvious differences. Fig. 8. shows the frontal lobe activation of HCs under three conditions. Red represents a strong activation of HbO, while yellow indicates that activation is not obvious. By comparing Fig. 7 (a) and Fig. 8 (a), we found that the right orbitofrontal cortex (ROFC) and left orbitofrontal cortex (LOFC) were both activated in MDD patients and HCs. However, for the MDD group, the activation of the ROFC was significantly stronger than that of the LOFC. By comparing Fig. 7 (b) and Fig. 8 (b), we can conclude that compared with HCs, the activation area of MDD patients is significantly reduced because depressed mood is associated with the bilateral ventrolateral PFC (VLPFC). We found that the activated state of the MDD group was significantly reduced under neutral conditions in the bilateral dorsolateral PFC (DLPFC).

Our result supports the findings from [49]; specifically, MDD subjects showed reduced functional connectivity in parts of the default mode network (DMN) compared with HCs. Fig. 7 (c) and Fig. 8 (c) show the HbO concentration changes in the MDD patients and HCs in terms of the fear emotion, and these changes are significantly different than those found for the happiness emotion. There were significant differences between the MDD patients and HCs in the activation region. MDD group activation was significantly reduced in the bilateral ventrolateral PFC (VLPFC), while there was apparent activation in the HCs. Based on all of the above results, it can be deduced that MDD patients had abnormal activation patterns compared with HCs [47], [52], [53], and depression may lead to abnormal blood oxygen metabolism in MDD patients.

TABLE VI
STRUCTURES AND PARAMETERS OF SIMPLE NEURAL NETWORKS

Network	Input	Hidden layers	Hidden neurons	Output
MNN	88	3	[10, 10, 10]	2
FNN	88	4	[10, 10, 10, 10]	2
CFNN	88	5	[10, 10, 10, 10, 10]	2
RNN	88	5	[10, 10, 10, 10, 10]	2

D. Simple Neural Networks

To determine the optimal feature combination that provides the best results, all possible single-feature, two-feature, three-feature and all-feature combinations using the statistical- and vector-based features were computed. All the statistical- and vector-based features were used to obtain classification accuracies for the two groups (MDD vs. HC) using a simple neural network.

In this study, we used four simple neural networks to perform classifications: a multilayer neural network (MNN), a feedforward neural network (FNN), a cascade forward neural network (CFNN), and a recurrent neural network (RNN). The network structures are shown in Table VI. The classification performance was evaluated using LOSO strategy. For the MNN, the training algorithm used was the scaled conjugate gradient (CG) method [54], and the performance was measured by the cross-entropy. For the FNN, CFNN and RNN, the training algorithm used was the Levenberg-Marquardt (LM) method [54], and the performance was measured by the mean squared error (MSE).

Table VII provides the accuracies of signal features using statistical- and vector-based features. The highest classification accuracies obtained using a single feature are 88.79% (happiness: RNN_AUC) and 98.61% (fear: CFNN_$|L|$) for the two types of features. Table VIII provides the accuracies of the two-feature combinations using the statistical- and vector-based features. The highest classification accuracies obtained using the two-feature combinations are 87.37% (fear: FNN_Mean and STD) and 99.78% (happiness: CFNN_ΔCOE and $|L|$). Table IX provides the accuracies of three-feature combinations using the statistical- and vector-based features. The highest classification accuracies obtained using the three-feature combinations are 90.51% (fear: CFNN_Mean, STD and Slope) and 99.91% (fear: RNN_ΔCBV, ΔCOE and $|L|$). Table X provides the accuracies for the all-feature combinations using the statistical- and vector-based features. The highest classification accuracies obtained using the all-feature combinations are 89.74% (fear: mean, STD, AUC and slope) and 99.94% (fear: ΔCBV, ΔCOE, $|L|$ and K) for the two types of features.

In conclusion, these results suggested that the best result was obtained for the fear condition. Therefore, there is a significant

TABLE VII
AVERAGE CLASSIFICATION ACCURACIES OF THE SIGNAL STATISTICAL- AND VECTOR-BASED FEATURES FOR THE MDD PATIENTS AND HCS

Single Feature	Happiness (%)				Calm (%)				Fear (%)			
	MNN	FNN	CFNN	RNN	MNN	FNN	CFNN	RNN	MNN	FNN	CFNN	RNN
Mean	59.42	66.03	72.19	77.89	54.38	63.94	76.10	78.67	68.74	72.72	**78.98**	76.54
STD	62.58	72.23	76.15	78.47	70.28	73.67	78.83	84.79	71.00	81.87	84.20	**88.76**
AUC	66.28	79.38	82.04	**88.79**	73.50	78.74	88.47	84.69	84.05	79.97	83.17	87.94
Slope	77.49	75.13	67.58	79.80	74.23	78.92	79.64	83.70	76.77	**88.51**	86.18	88.03
ΔCBV	93.49	94.98	93.53	94.34	91.55	93.22	5.48	90.45	96.51	93.66	94.964	**98.24**
ΔCOE	94.57	91.63	93.72	95.21	95.58	96.01	90.49	93.83	94.03	95.98	**96.72**	95.53
Magnitude of vector $\|L\|$	96.74	97.18	98.30	93.23	94.13	91.83	97.13	95.62	98.08	95.66	**98.61**	93.47
Angle (K)	84.31	83.62	**90.16**	87.58	81.00	87.816	84.30	89.24	83.20	90.023	85.09	88.10

* The bold values represent the maximum accuracy achieved in each row.

TABLE VIII
AVERAGE CLASSIFICATION ACCURACIES OF THE TWO-FEATURE COMBINATIONS FOR THE MDD PATIENTS AND HCS

Two-Feature Combination	Happiness (%)				Calm (%)				Fear (%)			
	MNN	FNN	CFNN	RNN	MNN	FNN	CFNN	RNN	MNN	FNN	CFNN	RNN
Mean and STD	74.35	83.65	83.58	87.83	71.79	85.00	69.35	86.60	86.53	**87.37**	81.21	85.19
Mean and AUC	77.37	78.07	**86.53**	79.67	71.08	72.50	79.48	79.73	65.57	76.47	69.48	81.02
Mean and Slope	72.69	**83.52**	66.47	77.11	71.02	66.92	69.42	81.08	67.17	81.02	70.19	79.42
STD and AUC	71.53	84.29	84.93	81.23	68.91	67.05	75.89	82.02	80.25	82.69	77.30	**85.76**
STD and Slope	63.83	77.94	71.79	77.30	70.38	71.73	74.67	77.24	80.75	82.50	81.21	**84.80**
AUC and Slope	71.53	76.41	70.19	81.21	79.55	77.30	67.94	69.51	81.01	77.24	**84.29**	81.08
ΔCBV and ΔCOE	96.60	93.68	**97.98**	97.90	90.92	92.44	95.94	94.47	93.65	94.92	97.87	96.89
ΔCBV and $\|L\|$	97.62	94.78	98.91	98.5	95.86	97.30	97.77	95.26	97.52	98.89	**99.58**	97.58
ΔCBV and K	96.41	97.96	96.85	98.68	95.17	96.95	95.29	98.58	97.59	98.01	96.53	**99.06**
ΔCOE and $\|L\|$	98.10	98.77	**99.78**	98.72	96.50	97.36	95.83	99.36	99.03	96.07	97.75	99.68
ΔCOE and K	96.76	98.46	98.04	99.07	98.78	96.64	98.58	99.10	98.67	99.09	**99.74**	99.34
$\|L\|$ and K	97.17	95.04	99.07	96.28	96.01	98.58	98.83	99.10	99.06	98.67	**99.20**	99.09

* The bold values represent the maximum accuracy achieved in each row.

TABLE IX
AVERAGE CLASSIFICATION ACCURACIES OF THE THREE-FEATURE COMBINATIONS FOR THE MDD PATIENTS AND HCS

Three-Feature Combination	Happiness (%)				Calm (%)				Fear (%)			
	MNN	FNN	CFNN	RNN	MNN	FNN	CFNN	RNN	MNN	FNN	CFNN	RNN
Mean, STD and AUC	78.84	74.16	82.69	82.56	70.83	75.06	79.03	78.97	73.52	84.29	89.67	**89.03**
Mean, STD and Slope	70.76	75.51	85.06	**85.76**	77.94	75.57	85.61	77.82	78.07	76.53	84.29	79.55
Mean, AUC and Slope	62.24	68.58	81.02	72.62	79.61	69.29	85.70	78.65	79.55	71.08	**85.89**	81.85
STD, AUC and Slope	68.71	72.25	**90.51**	79.35	69.55	73.58	88.07	78.78	69.61	77.37	86.34	85.43
ΔCBV, ΔCOE and $\|L\|$	94.09	99.78	99.86	98.91	97.52	97.36	99.37	98.94	96.27	98.52	99.75	**99.91**
ΔCBV, ΔCOE and K	99.04	99.07	99.77	**99.86**	99.10	98.58	99.69	99.71	99.29	98.67	98.09	99.73
ΔCBV, $\|L\|$ and K	99.04	99.07	99.44	98.96	98.82	98.77	99.10	98.58	98.67	99.09	99.82	**99.70**
ΔCOE, $\|L\|$ and K	99.07	99.04	99.78	99.69	96.71	98.58	98.31	99.35	99.09	98.67	**99.83**	99.70

* The bold values represent the maximum accuracy achieved in each row.

difference between the MDD patients and HCs in terms of negative emotions, and negative emotions play an important role in the distinction between MDD patients and HCs.

E. Feature Selection

In this study, we used the ReliefF algorithm to perform feature selection, and its classification accuracies are shown in Fig. 9 and Fig. 10. The results of feature selection with 6 different parameters (ref (5), ref (10), ref (15), ref (20), ref (25), ref (30)) were compared with those without feature selection. As can be seen from the figures, when the feature dimensions are reduced to 10 dimensions, there is better accuracy and fewer feature dimensions. Additionally, we performed simple feature fusion and machine learning classification (KNN, RF and SVM) of the 10-dimensional feature results, as shown in Table XI and Table XII.

Table XI shows the accuracy when the feature dimensions are reduced to 10 dimensions. For the statistical-based features, the highest accuracy is 83.52% (fear: CFNN_Ref (10)),

TABLE X
AVERAGE CLASSIFICATION ACCURACIES OF THE ALL-FEATURE COMBINATIONS FOR THE MDD PATIENTS AND HCS

All-Feature Combination	Happiness (%)				Calm (%)				Fear (%)			
	MNN	FNN	CFNN	RNN	MNN	FNN	CFNN	RNN	MNN	FNN	CFNN	RNN
Mean, STD, AUC and Slope	74.16	74.03	87.43	74.67	66.41	69.42	84.50	78.14	78.714	78.91	81.92	**89.74**
ΔCBV, ΔCOE, $\|L\|$ and K	99.07	99.04	99.09	99.89	98.58	99.10	99.75	98.90	99.72	98.67	**99.94**	99.86

* The bold values represent the maximum accuracy achieved in each row.

TABLE XI
RESULTS OF FEATURE SELECTION AND FEATURE FUSION

Feature selection	Happiness (%)				Calm (%)				Fear (%)			
	MNN	FNN	CFNN	RNN	MNN	FNN	CFNN	RNN	MNN	FNN	CFNN	RNN
Statistical Feature–Ref (10)	66.34	67.88	75.51	81.98	62.37	77.30	78.78	75.32	72.65	79.10	**83.52**	78.01
Vector Feature–Ref (10)	84.06	82.96	91.99	87.95	83.95	85.04	89.24	80.46	89.52	90.28	**92.33**	91.47
Feature Fusion	78.53	80.43	83.51	81.88	74.42	79.98	90.01	80.77	80.55	83.72	**87.66**	85.32

TABLE XII
RESULTS OF MACHINE LEARNING

Feature selection	Happiness (%)			Calm (%)			Fear (%)		
	KNN	RF	SVM	KNN	RF	SVM	KNN	RF	SVM
Statistical Feature–Ref (10)	69.32	70.88	73.24	67.55	71.32	70.89	71.54	76.54	**79.67**
Vector Feature–Ref (10)	79.88	78.90	82.45	77.26	76.60	79.67	79.70	83.92	**86.60**

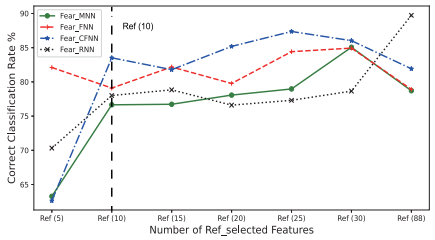

Fig. 9. Results of the statistical-based feature using the ReliefF feature selection algorithm.

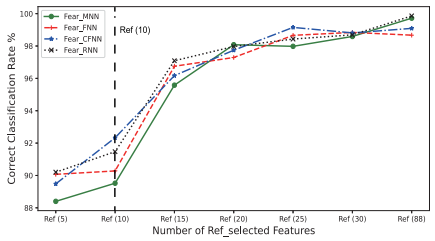

Fig. 10. Results of the vector-based feature using the ReliefF feature selection algorithm.

and for the vector-based features, the highest accuracy is 91.99% (fear: CFNN_Ref (10)). Table XII shows that the highest accuracy of machine learning when the feature dimensions are reduced to 10 dimensions is 79.67% (fear: SVM) and 86.60% (fear: SVM). In addition, Table XIII shows the top 10 features we obtained. These features show that the

TABLE XIII
RESULTS FOR THE STATISTICAL- AND VECTOR-BASED FEATURES USING THE RELIEFF FEATURE SELECTION ALGORITHM AND THE TOP 10 FEATURES OBTAINED FOR EACH CLASS

Feature selection	Happiness	Fear
Statistical feature	Ch16_AUC, Ch15_AUC	Ch22_AUC, Ch22_STD
	Ch2_Mean, Ch17_AUC	Ch20_AUC, Ch7_Mean
	Ch9_AUC, Ch7_AUC	Ch20_STD, Ch21_AUC
	Ch1_AUC, Ch1_Mean	Ch19_AUC, Ch15_AUC
	Ch19_Mean, Ch10_Mean	Ch13_AUC, CH8_AUC
Vector feature	Ch14_K, Ch4_K	Ch15_K, Ch14_K
	Ch10_K, Ch6_ΔCBV	Ch10_ΔCOE, Ch13_K
	Ch19_K, Ch5_K	Ch11_K, Ch1_ΔCOE
	Ch6_$\|L\|$, Ch22_K	Ch9_ΔCBV, Ch4_$\|L\|$
	Ch1_K, Ch11_K	Ch22_K, Ch19_K

abovementioned combinations can also be effectively used to achieve enhanced classification accuracies.

V. DISCUSSION

The present study investigated fNIRS-based MDD recognition. Four different methods, namely, correlation analysis of the oxygen index and scales, resting-state analysis, activation analysis and simultaneous neural network recognition, were used for quantitative recognition of MDD patients. The response patterns for different emotion classes were characterized by computing the Pearson correlation coefficients between

the HbO/HbR responses of each individual fNIRS channel and four scale scores. The MDD and HC groups had significant differences in terms of the AIS scores. We speculate that MDD patients often have insomnia, which will affect their blood oxygen metabolism for a long time. Kawano *et al.* [48] investigated the relationship between recorded blood flow and depression severity assessed using the Hamilton depression scale in patients with various psychiatric disorders, and they found that the severity of depression was negatively correlated with the integral value of blood flow in the frontal lobe, irrespective of psychiatric diagnosis (f=5.94, P=0.02). Our results support blood flow in the frontal lobe as an potential biomarker of depression severity across various psychiatric disorders.

By quantitatively evaluating the functional connectivity, we found that MDD patients exhibit aberrant functional connectivity compared with HCs. In Rosenbaum's study, subjects with depression showed reduced functional connectivity in parts of the DMN compared with HCs. The results suggest that MDD damages the local connectivity of the functional brain networks of patients, which is consistent with the results of earlier studies [55].

Previous fNIRS studies have reported reduced oxygenation changes in the PFC during cognitive tasks in patients with MDD [56]. One study used image stimuli to induce very pleasant, neutral, and very unpleasant emotional states, and it was found that negative emotion was accompanied by an increase in HbO in the bilateral VLPFC. Nevertheless, positive emotion showed a decrease in HbO in the left dorsolateral PFC [57]. However, another music therapy-based study showed that the MDD group exhibited significant activation in the DLPFC, orbitofrontal cortex (OFC) and ventromedial prefrontal cortex (VMPFC) after music therapy [3]. In the present study, the reduction in the HbO concentration in the PFC subregions is consistent with previous fNIRS studies in humans [2], and we found significant differences between patients with MDD and HCs in terms of the activation region. The activated state of the MDD group was significantly reduced under neutral conditions in the bilateral DLPFC, and the blood oxygen metabolism level in the bilateral VLPFC was significantly reduced. Based on all of the above results, it could be deduced that MDD patients have abnormal activation patterns compared with HCs.

As summarized in Tables VII-X, the statistical-based features achieved an accuracy of 89.74%. However, the classification performance of the vector-based features demonstrated significant improvement compared with the former, achieving an accuracy of 99.94%. In addition, the result of the ReliefF feature selection algorithm indicates that by using only 10-dimensional features, we can also obtain better results.

These results all indicate that there are great differences between MDD patients and HCs in different aspects. The innovations of this paper are as follows: (1) The differences in brain activity between MDD patients and HCs were analyzed from different perspectives, providing some neuroscience evidence for our subsequent classification. (2) We tried to use correlation analysis to assess the association between the blood oxygen index and scales and found that there was a significant negative correlation between HbO and sleep status in MDD patients. (3) Two types of features, namely, statistical-based features and vector-based features, were extracted from our dataset. Moreover, good results were obtained using four simple neural networks. Through the method of feature selection, we found that when the feature dimensions are reduced to 10 dimensions, the highest accuracy is 83.52% and 91.99% for statistical- and vector-based features, respectively. We also identified the AUC and angle K as specific neuromarkers for predicting MDD across specific depression-related regions of the PFC.

In the future, we will aim to employ the concurrent EEG+fNIRS method, the decoding accuracy of which has been shown to be greater than that of its subsystems. We are now developing a set of portable EEG+fNIRS devices for medical diagnosis and rehabilitation engineering, and we will aim to identify a new type of neurovascular feature derived from hybrid data. Beyond these objectives, we will attempt to provide some optimal channel selection methods to reduce the number of source and detector optodes while retaining the classification performance. Additionally, to translate these findings to the clinical diagnosis of depression, more extensive research with a larger sample size involving both sexes must be performed.

REFERENCES

[1] R. C. Kessler and E. J. Bromet, "The epidemiology of depression across cultures," *Annu. Rev. Public Health*, vol. 34, no. 1, pp. 119–138, Mar. 2013.

[2] Baik *et al.*, "Prefrontal asymmetry during cognitive tasks and its relationship with suicide ideation in major depressive disorder: An fNIRS study," *Diagnostics*, vol. 9, no. 4, p. 193, Nov. 2019.

[3] K. Feng *et al.*, "Effects of music therapy on major depressive disorder: A study of prefrontal hemodynamic functions using fNIRS," *Psychiatry Res.*, vol. 275, pp. 86–93, May 2019.

[4] M. F. Folstein, S. E. Folstein, and P. R. McHugh, "Mini-mental state: A practical method for grading the cognitive state of patients for the clinician," *J. Psychiatric Res.*, vol. 12, no. 3, pp. 189–198, Nov. 1975.

[5] M. Hamilton, "A rating scale for depression," *J. Neurol., Neurosurg., Psychiatry*, vol. 23, no. 1, p. 56, 1960.

[6] R. Takizawa *et al.*, "Neuroimaging-aided differential diagnosis of the depressive state," *NeuroImage*, vol. 85, pp. 498–507, Jan. 2014.

[7] C.-H. Lai, "Promising neuroimaging biomarkers in depression," *Psychiatry Invest.*, vol. 16, no. 9, p. 662, 2019.

[8] S. Olbrich and M. Arns, "EEG biomarkers in major depressive disorder: Discriminative power and prediction of treatment response," *Int. Rev. Psychiatry*, vol. 25, no. 5, pp. 604–618, Oct. 2013.

[9] J. Shen, X. Zhang, B. Hu, G. Wang, Z. Ding, and B. Hu, "An improved empirical mode decomposition of electroencephalogram signals for depression detection," *IEEE Trans. Affect. Comput.*, early access, Aug. 14, 2020, doi: 10.1109/TAFFC.2019.2934412.

[10] K. Domschke *et al.*, "Magnetoencephalographic correlates of emotional processing in major depression before and after pharmacological treatment," *Int. J. Neuropsychopharmacol.*, vol. 19, no. 2, Feb. 2016, Art. no. pyv093.

[11] Z. Yao *et al.*, "Structural alterations of the brain preceded functional alterations in major depressive disorder patients: Evidence from multimodal connectivity," *J. Affect. Disorders*, vol. 253, pp. 107–117, Jun. 2019.

[12] J. Mota Pereira and D. Fonte, "Pets enhance antidepressant pharmacotherapy effects in patients with treatment resistant major depressive disorder," *J. Psychiatric Res.*, vol. 104, pp. 108–113, Sep. 2018.

[13] B. Hu *et al.*, "Emotion regulating attentional control abnormalities in major depressive disorder: An event-related potential study," *Sci. Rep.*, vol. 7, no. 1, Dec. 2017, Art. no. 13530.

[14] C. Park *et al.*, "The neural systems of emotion regulation and abnormalities in major depressive disorder," *Behav. Brain Res.*, vol. 367, pp. 181–188, Jul. 2019.

[15] F. F. Jöbsis, "Noninvasive, infrared monitoring of cerebral and myocardial oxygen sufficiency and circulatory parameters," *Science*, vol. 198, no. 4323, pp. 1264–1267, 1977.

[16] F. Wang, M. Mao, L. Duan, Y. Huang, Z. Li, and C. Zhu, "Intersession instability in fNIRS-based emotion recognition," *IEEE Trans. Neural Syst. Rehabil. Eng.*, vol. 26, no. 7, pp. 1324–1333, Jul. 2018.

[17] J. An, S. H. Lee, Y. J. Lee, S. H. Jin, and G. Jang, "Applications of functional near infrared spectroscopy as a brain optical imaging modality for rehabilitation," in *Proc. Int. Symp. Optomechatron. Technol.*, 2014, pp. 50–56.

[18] H. Tomioka *et al.*, "A longitudinal functional neuroimaging study in medication-Naïve depression after antidepressant treatment," *PLoS ONE*, vol. 10, no. 3, Mar. 2015, Art. no. e0120828.

[19] X. Liu *et al.*, "Relationship between the prefrontal function and the severity of the emotional symptoms during a verbal fluency task in patients with major depressive disorder: A multi-channel NIRS study," *Prog. Neuro-Psychopharmacol. Biol. Psychiatry*, vol. 54, pp. 114–121, Oct. 2014.

[20] H. Akashi, N. Tsujii, W. Mikawa, T. Adachi, E. Kirime, and O. Shirakawa, "Prefrontal cortex activation is associated with a discrepancy between self and observer-rated depression severities of major depressive disorder: A multichannel near-infrared spectroscopy study," *J. Affect. Disorders*, vol. 174, pp. 165–172, Mar. 2015.

[21] S. F. Husain *et al.*, "Validating a functional near-infrared spectroscopy diagnostic paradigm for major depressive disorder," *Sci. Rep.*, vol. 10, no. 1, Dec. 2020, Art. no. 9740.

[22] H. Zhang *et al.*, "Near-infrared spectroscopy for examination of prefrontal activation during cognitive tasks in patients with major depressive disorder: A meta-analysis of observational studies," *Psychiatry Clin. Neurosci.*, vol. 69, no. 1, pp. 22–33, Jan. 2015.

[23] T. Matsubara *et al.*, "Prefrontal activation in response to emotional words in patients with bipolar disorder and major depressive disorder," *NeuroImage*, vol. 85, no. 2, pp. 489–497, 2014.

[24] Y. Zhu *et al.*, "Classifying major depressive disorder using fNIRS during motor rehabilitation," *IEEE Trans. Neural Syst. Rehabil. Eng.*, vol. 28, no. 4, pp. 961–969, Apr. 2020.

[25] T. Ma *et al.*, "Distinguishing bipolar depression from major depressive disorder using fNIRS and deep neural network," *Prog. Electromagn. Res.*, vol. 169, pp. 73–86, 2020.

[26] Y. Zhu and M. S. R. K. Mehta, "Machine learning approach on frontal lobe activity to assess depression in adults: Implications for rehabilitation outcomes," in *Proc. Int. Symp. Wearable Robot. Rehabil. (WeRob)*, Nov. 2017, pp. 1–2.

[27] R. Zimmermann *et al.*, "Detection of motor execution using a hybrid fNIRS-biosignal BCI: A feasibility study," *J. Neuroeng. Rehabil.*, vol. 10, no. 1, pp. 1–15, 2013.

[28] R. A. Khan, N. Naseer, N. K. Qureshi, F. M. Noori, H. Nazeer, and M. U. Khan, "FNIRS-based neurorobotic interface for gait rehabilitation," *J. NeuroEng. Rehabil.*, vol. 15, no. 1, pp. 1–17, Dec. 2018.

[29] S. Xu *et al.*, "Attention based multi-level co-occurrence graph convolutional LSTM for 3D action recognition," *IEEE Internet Things J.*, early access, Dec. 8, 2020, doi: 10.1109/JIOT.2020.3042986.

[30] H. Nazeer *et al.*, "Enhancing classification accuracy of fNIRS-BCI using features acquired from vector-based phase analysis," *J. Neural Eng.*, vol. 17, no. 5, Oct. 2020, Art. no. 056025.

[31] K. Tai and T. Chau, "Single-trial classification of NIRS signals during emotional induction tasks: Towards a corporeal machine interface," *J. NeuroEng. Rehabil.*, vol. 6, no. 1, pp. 1–14, Dec. 2009.

[32] T. J. Huppert, S. G. Diamond, M. A. Franceschini, and D. A. Boas, "Homer: A review of time-series analysis methods for near-infrared spectroscopy of the brain," *Appl. Opt.*, vol. 48, no. 10, pp. 280–298, 2009.

[33] D. Delpy and M. Cope, "Quantification in tissue near–infrared spectroscopy," *Philos. Trans. Roy. Soc. London. Ser. B, Biol. Sci.*, vol. 352, no. 1354, pp. 649–659, 1997.

[34] F. Klein and C. Kranczioch, "Signal processing in fNIRS: A case for the removal of systemic activity for single trial data," *Frontiers Hum. Neurosci.*, vol. 13, p. 331, Sep. 2019.

[35] T. Nozawa and T. Kondo, "A comparison of artifact reduction methods for real-time analysis of fNIRS data," *Proc. Symp. Hum. Interface Manage. Inf. Inf. Interact.*, vol. 5618, 2009, pp. 413–422.

[36] R. J. Cooper *et al.*, "A systematic comparison of motion artifact correction techniques for functional near-infrared spectroscopy," *Frontiers Neurosci.*, vol. 6, p. 147, Oct. 2012.

[37] M. A. Yücel *et al.*, "Mayer waves reduce the accuracy of estimated hemodynamic response functions in functional near-infrared spectroscopy," *Biomed. Opt. Exp.*, vol. 7, no. 8, pp. 3078–3088, 2016.

[38] K. J. Friston, A. P. Holmes, K. J. Worsley, J.-P. Poline, C. D. Frith, and R. S. Frackowiak, "Statistical parametric maps in functional imaging: A general linear approach," *Hum. Brain Mapping*, vol. 2, no. 4, pp. 189–210, 1994.

[39] J. Ye, S. Tak, K. Jang, J. Jung, and J. Jang, "NIRS-SPM: Statistical parametric mapping for near-infrared spectroscopy," *NeuroImage*, vol. 44, no. 2, pp. 428–447, Jan. 2009.

[40] N. Naseer, M. J. Hong, and K.-S. Hong, "Online binary decision decoding using functional near-infrared spectroscopy for the development of brain–computer interface," *Exp. Brain Res.*, vol. 232, no. 2, pp. 555–564, Feb. 2014.

[41] K.-S. Hong, N. Naseer, and Y.-H. Kim, "Classification of prefrontal and motor cortex signals for three-class fNIRS–BCI," *Neurosci. Lett.*, vol. 587, no. 1, pp. 87–92, Feb. 2015.

[42] K. Yoshino and T. Kato, "Vector-based phase classification of initial dips during word listening using near-infrared spectroscopy," *NeuroRep.*, vol. 23, no. 16, pp. 947–951, 2012.

[43] K.-S. Hong and N. Naseer, "Reduction of delay in detecting initial dips from functional near-infrared spectroscopy signals using vector-based phase analysis," *Int. J. Neural Syst.*, vol. 26, no. 3, May 2016, Art. no. 1650012.

[44] Y. Huang, P. J. McCullagh, and N. D. Black, "An optimization of ReliefF for classification in large datasets," *Data Knowl. Eng.*, vol. 68, no. 11, pp. 1348–1356, Nov. 2009.

[45] D. Nutt, S. Wilson, and L. Paterson, "Sleep disorders as core symptoms of depression," *Dialogues Clin. Neuro.*, vol. 10, no. 3, pp. 329–336, 2008.

[46] F. Yang *et al.*, "Internet of Things enabled data fusion method for sleep healthcare applications," *IEEE Internet Things J.*, early access, Mar. 22, 2021, doi: 10.1109/JIOT.2021.3067905.

[47] T. Noda *et al.*, "Frontal and right temporal activations correlate negatively with depression severity during verbal fluency task: A multi-channel near-infrared spectroscopy study," *J. Psychiatric Res.*, vol. 46, no. 7, pp. 905–912, Jul. 2012.

[48] M. Kawano *et al.*, "Correlation between frontal lobe oxy-hemoglobin and severity of depression assessed using near-infrared spectroscopy," *J. Affect. Disorders*, vol. 205, pp. 154–158, Nov. 2016.

[49] G. S. Alexopoulos, M. J. Hoptman, D. Kanellopoulos, C. F. Murphy, K. O. Lim, and F. M. Gunning, "Functional connectivity in the cognitive control network and the default mode network in late-life depression," *J. Affect. Disorders*, vol. 139, no. 1, pp. 56–65, Jun. 2012.

[50] Y. Chen, C. Wang, X. Zhu, Y. Tan, and Y. Zhong, "Aberrant connectivity within the default mode network in first-episode, treatment-naive major depressive disorder," *J. Affect. Disorders*, vol. 183, pp. 49–56, Sep. 2015.

[51] H. Doi, S. Nishitani, and K. Shinohara, "NIRS as a tool for assaying emotional function in the prefrontal cortex," *Frontiers Hum. Neurosci.*, vol. 7, no. 2, p. 770, Nov. 2013.

[52] M. Schecklmann *et al.*, "Reduced prefrontal oxygenation during object and spatial visual working memory in unpolar and bipolar depression," *Psychiatry Res., Neuroimag.*, vol. 194, no. 3, pp. 378–384, Dec. 2011.

[53] G. J. Siegle, W. Thompson, C. S. Carter, S. R. Steinhauer, and M. E. Thase, "Increased amygdala and decreased dorsolateral prefrontal BOLD responses in unipolar depression: Related and independent features," *Biol. Psychiatry*, vol. 61, no. 2, pp. 198–209, Jan. 2007.

[54] K. Madsen, H. B. Nielsen, and O. Tingleff, "Methods for non–linear least squares problems," Soc. Ind. Appl. Math., Lyngby, Denmark, Tech. Rep., 2004, p. 56.

[55] X. Li *et al.*, "A resting-state brain functional network study in MDD based on minimum spanning tree analysis and the hierarchical clustering," *Complexity*, vol. 2017, Jul. 2017, Art. no. 9514369.

[56] J. Leon-Carrion *et al.*, "Differential time course and intensity of PFC activation for men and women in response to emotional stimuli: A functional near-infrared spectroscopy (fNIRS) study," *Neurosci. Lett.*, vol. 403, nos. 1–2, pp. 90–95, Jul. 2006.

[57] Y. Hoshi *et al.*, "Recognition of human emotions from cerebral blood flow changes in the frontal region: A study with event-related near-infrared spectroscopy," *J. Neuroimag.*, vol. 21, no. 2, pp. 94–101, Apr. 2011.